

# Fermi National Accelerator Laboratory

FERMILAB-Pub-81/59  
1100.050  
(Submitted to Nucl. Instrum. Methods)

ABSORBED DOSE MEASUREMENTS EXTERNAL  
TO THICK SHIELDING AT A HIGH ENERGY PROTON ACCELERATOR:  
COMPARISON WITH MONTE-CARLO CALCULATIONS

J. D. Cossairt, N. V. Mokhov,\* and C. T. Murphy

September 1981

---

\*Permanent address: Institute for High Energy Physics,  
Serpuukhov, USSR.

ABSORBED DOSE MEASUREMENTS EXTERNAL  
TO THICK SHIELDING AT A HIGH ENERGY  
PROTON ACCELERATOR: COMPARISON  
WITH MONTE-CARLO CALCULATIONS

J. D. Cossairt, N. V. Mokhov,\* and C. T. Murphy  
Fermilab , Batavia, IL. 60510, U.S.A.

Abstract

The design of efficient biological shielding at a 400 GeV proton synchrotron is often done using Monte Carlo computer calculations. Several test cases involving lateral concrete and soil shields up to 660 cm thick were selected according to a criterion of simplicity. Measurements of absorbed dose rates were done using tissue equivalent ion and proportional chambers. Agreement typically within a factor of three is obtained with Monte-Carlo calculations using the program CASIM developed at Fermilab. No evidence was found for any systematic dependence of the degree of agreement upon the thickness of the shield.

\*Permanent Address: Institute for High Energy Physics,  
Serpuukhov, USSR.

## 1. Introduction and General Discussion of Technique

The design of shielding for high energy proton accelerators must be done efficiently for economic reasons while also assuring safety of personnel and the general public. At Fermilab, Monte-Carlo techniques have been employed for a number of years using the hadronic cascade code CASIM, and its derivatives, developed by A. Van Ginneken and described elsewhere.<sup>1,2</sup> This code is used to calculate the propagation of hadronic cascades and associated quantities of practical interest such as soil activation, energy deposition in thick targets and calorimeters, and absorbed dose rates. The absorbed dose rates are usually converted to dose equivalent rates using average quality factors. The code has previously been tested in its ability to predict activation of foils and energy deposition for targets of relatively small dimensions.<sup>3,4</sup> Very little testing of the code up to the present applies to shielding of relatively large dimensions used for personnel protection at Fermilab. Because of the enormous cost of shielding the 1000 GeV accelerator (the Tevatron) presently being installed, it has become obvious that efficient lateral shielding design is necessary.

In this work, several test cases were selected according to criteria given below. The absorbed dose rates were measured for these cases and compared with appropriate Monte-Carlo calculations. Absorbed dose was chosen as a quantity for measurement because it is a purely physical quantity (1 rad equals 100 ergs/gram in tissue) which can be reliably measured by tissue equivalent ionization and proportional chambers in the expected spectrum.<sup>5</sup> The availability of portable versions of these chambers facilitates use on shielding berms remote from electrical power outlets with a minimum of set up time. In the present work all instruments were calibrated within one day of their use both before and after the measurement.

Lateral shielding cases were studied because forward angle situations would involve contamination from muon radiation fields which would add uncertainties to the Monte-Carlo calculations. Such fields can, however, be modeled using a modification of the present code.<sup>6</sup> Other criteria used to select cases for study were:

A) The geometry must be verifiable by tape measurements or alignment surveys.

B) Intensity monitoring and beam location must be

well understood especially for cases where the beam is artificially dumped, for example, by turning off a magnet.

C) The geometry should be simple enough to be modeled by the FORTRAN subroutine used in the Monte-Carlo calculations.

In practice these criteria limit the present work to direct dumping and eliminated cases of scraping losses because of the sensitivity of such losses to beam direction, spot size and profile (which are usually impossible to measure with sufficient precision).

The Monte-Carlo calculations were carried out using CASIM. The geometry was entered into the calculation using the FORTRAN subroutine HITORM (normally supplied by the user for a specific case as was done here). In all cases beam shapes were modeled as being rectangular shapes uniformly illuminated with widths set equal to the FWHM of the beam spot as measured on beam profile monitors. The effect of neglecting Gaussian tails in the modeling of the beam profiles is expected to be negligible. Beam targeting angles were accurately included in the calculations.

Of course, the densities of the various materials used is crucial. The density of the metals are well known. For the concrete  $2.4 \text{ g/cm}^3$  was used while for soil the value of  $2.24 \text{ g/cm}^3$  was used. This value, a wet density, has been verified by soil borings through compacted berms. If this value is used instead of the more conventional dry density of  $2.1 \text{ g/cm}^3$ , the results for a 460 cm thick soil shield differ by a factor of two based upon an absorption length of  $92 \text{ g/cm}^2$  for concrete (soil).<sup>7</sup> In all cases soil was considered to have the same composition as concrete, both having an average atomic number of 11.0 and average atomic mass of 23.0.

One important parameter is the factor used to convert the primary output of the program of stars (nuclear interactions) per  $\text{cm}^3$  per incident hadron to rads of absorbed dose per hadron. The method for obtaining such a factor is described in detail in refs. 2 and 8 where it is shown that its value depends upon the location within the shield and upon the material. This is, of course, a reflection of the variation of the spectrum with location. However, the variation of this factor (and the spectrum) with location becomes very small after about 150 cm of concrete so that for such an equilibrium spectrum, a value of  $1.5 \text{ } \mu\text{rad}/(\text{star}\cdot\text{cm}^{-3})$  is a good one. Scaling by the ratio of densities leads one to the value of  $1.6 \text{ } \mu\text{rad}/(\text{star}\cdot\text{cm}^{-3})$

for soil which was used here for shields sufficiently thick for this approach to be valid. As was done in refs. 2 and 8, a momentum threshold of 0.3 GeV/c was employed below which the hadrons were not followed.

Before we discuss the individual cases, it should be noted that the modeling of the geometry as reported in detail below is simplified in some ways. For example, for thick soil shields, rectangular geometry is correctly described inside enclosures while cylindrical approximations are made to enclosure walls and soil shield. This serves a two-fold purpose of simulating the methods of a relatively casual user of the code and also reducing statistical errors of the calculation by effectively increasing the solid angle. Test runs using more correct rectangular geometries agree within statistical errors with the cylindrical approximations.

## 2. Specific Cases Studied

The four specific test cases studied here are described in this section. For each case the geometry, and beam loss mechanism are described in detail. The approximation to the geometry used in the Monte-Carlo calculations is also

described. The cases will be discussed here in order of increasing shielding thicknesses.

Case A: Measurement at 260 g/cm<sup>2</sup> and 340 g/cm<sup>2</sup>

The measurement utilized the beam dump for Experiment 577 in the M6E beam line at the Meson Laboratory on June 13, 1980. Fig. 1 and fig. 2 show the geometry of the beam dump. A 200 GeV secondary hadron beam consisting mostly of  $\pi^-$  at intensities of approximately  $5 \times 10^6$ /pulse, 14 sec. cycle time was incident on this beam dump at the location shown at an angle of 10 milliradians to the east of perpendicular. The beam was confined to a spot approximately 2.5 cm diameter (FWHM) as measured by a SWIC (segmented wire ionization chamber) immediately upstream of the dump. The beam intensity was measured using a pair of scintillation paddles in coincidence monitored by Experiment 577 for this same purpose.

The absorbed dose was measured using a pair of tissue equivalent ion chambers<sup>9</sup> (Fermilab "Chipmunks") which incorporate a digitizer producing a count on a scaler per 0.5 microrad of absorbed dose. These detectors contain built in check sources (2 microcuries of <sup>137</sup>Cs) and were

located near low level radioactive materials (components of the beam dump). Thus a beam-off background measurement was performed and found to be 24  $\mu$ rads/12 minutes.

In the CASIM calculation, the geometry was modeled as shown in fig. 2. Two separate calculations accumulating 100000 stars each were performed. A different random number initial value (seed) was used in the second calculation with no significant differences due to the very good statistics obtained.

#### Case B: Measurement at 1116 g/cm<sup>2</sup>

This measurement involved dumping the primary proton beam on the end of an aluminum cylinder 20.3 cm diameter by 307 cm long in a tunnel leading to the P-Center pretarget area in the Proton Laboratory. For this measurement 350 GeV protons extracted in a slow spill of 1.5 sec duration at an intensity of about  $3 \times 10^{10}$  per pulse were used on June 19, 1980. The geometry is shown in fig. 3. The beam intensity was measured for each pulse using a secondary emission monitor (SEM) located 180 cm upstream of the aluminum. The calibration of the SEM was known from a recent foil activation calibration. A cross calibration of this SEM

with another SEM further upstream and comparisons of SWIC profiles places a limit of 15 per cent on any effect of backscatter upon the SEM readings. It was also feared that scraping losses on upstream beam transport magnets would cause serious backgrounds in the measurements so a test was done during the measurement with all the beam deliberately dumped on these magnets with negligible effects on the results.

The beam size was measured to be about 3 cm (horizontal FWHM) by 1 cm (FWHM) at the beam plug. The beam was approximately perpendicular to the beam plug.

Absorbed dose rates were measured at the above ground location indicated in fig. 3 using a portable tissue equivalent ionization ratemeter (TEIR) in integrate mode (used for verification of readings) and a portable tissue equivalent proportional chamber (HPI 1010).<sup>10</sup> The two meters agreed with each other within scale reading error (0.2  $\mu$ rads). A scan was done above the axis of the beam. At the approximate maximum of the cascade, a scan perpendicular to the beam verified centering with respect to the beam line.

The geometry as modeled is shown in fig 4. In this case and in Cases C and D, the longitudinal coordinate  $Z$  is measured along the axis of the beam with the origin at the

location of bombardment of the target. In fig. 4 the cylindrical approximation mentioned above is shown. Three computer runs with different random number seeds were made, each accumulating 300000 stars.

#### Case C: Measurement at $1339 \text{ g/cm}^2$

On June 19, 1980 a measurement was carried out in which the primary proton beam at 350 GeV was dumped on a closed horizontal collimator in the P-Center beam line (Enclosure H) in the Proton area under slow spill conditions. The above ground absorbed dose rates were measured above the shielding berm for this enclosure using the same portable instruments as in Case B. The actual geometry is shown in fig. 5. Approximately 400 cm downstream of the beginning of the collimator, the top of the berm decreases in elevation by about 200 cm in the next 400 cm along the Z axis.

The intensity was measured by averaging over 10 pulses prior to the measurement under conditions of good stability and found to be  $2.92 \times 10^{11}$  protons per pulse on the SEM used in Case B. Directly after this intensity measurement the magnet string immediately upstream (MH 322) was turned off and the collimator was closed and rotated so that the

beam did not aim directly at the crack in the collimator. The detailed geometry of the targeting is shown in fig. 6. At this point the protons were being dumped on the closed and rotated collimator while the absorbed dose measurements were being made over approximately a 12 minute period. During this period the SEM was blocked by the closed collimator. Intensity variations were sensed by checking the intensity of the accelerator, the intensity of other extracted beams, and the size of the beam profile measured on a SWIC upstream of the collimator. After the measurement was completed, the original operating conditions were restored and the SEM reading taken over 5 pulses and found to average  $3.04 \times 10^{11}$  protons per pulse. This was taken to be confirmation that no serious intensity variations (less than 10 per cent) occurred during the measurements. The SWIC profiles indicated that this variation was less than 7 per cent. In addition, the backgrounds were measured with all 3 beams (P-East, P-West, and P-Center) being transported normally through this enclosure to look for sources from possible scraping of the other 2 beam lines. The background was less than 0.1 microrad per pulse at all locations and thus is not a significant source of error. A scan was made perpendicular to the beam direction to establish the center line.

The Monte-Carlo modeling was done as shown in fig. 7. The beam was made incident at the 11.7 milliradian angle shown in fig. 6 in order to simulate the rotation of the collimator. This allowed the axis of the collimator to be the longitudinal axis of the geometry. Calculations with three different random number seeds each accumulating 200000 stars were done.

#### Case D: Measurement at 1608 g/cm<sup>2</sup>

In this measurement, the thickest shield studied here, the geometry of fig. 8 was involved. The target was a rectangular iron plug 12.7 cm x 12.7 cm x 325 cm long shielded by the concrete walls of Enclosure C in the Accelerator Switchyard (Meson area beam line) and a large soil shield. A primary proton beam at 350 GeV in a spot about 10 mm FWHM (both horizontal and vertical) was centered on this beam plug and perpendicular to it. The average beam intensity was  $1.1 \times 10^{13}$  protons per pulse (1.5 second spill) as measured by the Main Ring torroid (all extracted protons being sent down this beam line during a studies period). The assumption that most of this beam reached the target was supported by small values of loss monitor readings. The irradiation occurred over approximately an 8 minute period.

The absorbed dose rate was measured on top of the shielding berm above this enclosure using both the TEIR and HPI 1010 instruments. A scan was made perpendicular to the beam direction in order to establish the center line.

Fig. 9 shows the geometry used in the Monte-Carlo calculations to model this geometry. In this case two different random number seeds were used in runs accumulating 200000 stars each. A third calculation was done using one of these same seeds and accumulating 400000 stars.

### 3. Results

In this section the results of the absorbed dose measurements will be presented and compared with the Monte-Carlo calculations for each separate case described above. Special problems associated with each test case will be highlighted.

Case A: For this case the measurements were only done at 2 discrete points which have been identified as location A1 and location A2. The absorbed dose rates at these locations were:

Location A1: 59.1  $\mu\text{rad}/10^7$  hadrons

Location A2: 25.5  $\mu\text{rad}/10^7$  hadrons

For this case of relatively thin shielding it would be inaccurate to assume that an equilibrium spectrum is present at the detector locations. This is particularly true at location A1 involving an iron shield followed by only a little over one absorption length of concrete. Location A2 involves iron followed by about 2 absorption lengths of concrete which may be sufficient to develop a nearly equilibrium spectrum, according to ref. 8. For this case ref. 2 (assuming a solid concrete shield) gives a conversion factor of 2.6  $\mu\text{rad}/\text{star}\cdot\text{cm}^3$ . Averaging the CASIM results over the four volume bins closest to Location A2 and multiplying by this factor was used to obtain the CASIM estimate.

For location A1, a prescription given for such cases in ref. 8 was used to convert the star density calculated at Location A1 (again averaging over the four nearest volume bins) to an equivalent one in a solid iron shield. Ref. 2 was then used to obtain a conversion factor of 5.5  $\mu\text{rad}/\text{star}\cdot\text{cm}^3$ .

Using these methods, the CASIM calculations yield:

Location A1:  $72 \pm 3$  rad/ $10^7$  hadrons

Location A2:  $26 \pm 7$  rad/ $10^7$  hadrons

where the errors are the statistical ones in the Monte-Carlo calculation. The agreement in this case is then quite good.

Case B: In this case a longitudinal (along the beam line) scan was made. Fig. 10 shows the data plotted as a function of longitudinal coordinate Z superimposed upon the three CASIM calculations. The scatter of the data points is indicative of the errors associated with the absorbed dose measurement. Each data point represents a measurement during a different beam spill. The differences between the three CASIM calculations is indicative of the errors involved in the calculations. These differences are similar in magnitude to the statistical errors given as output by the code. The actual calculations included dipole magnets downstream of these to insure that any backscatter was properly included. The effect of these magnets upon the results was minimal. The conversion factor for an equilibrium spectrum external to a soil shield for absorbed dose ( $1.6 \mu\text{rad}/\text{star} \cdot \text{cm}^3$ ) was used in this and Cases C and D.

As one can see, there are significant differences among the three calculations and the difference between measurement and calculation is especially pronounced at large values of  $Z$  (where the statistical errors in the calculation are larger). The ratio of measurements to calculations ranges from a factor of two to a factor of 0.25. An independent calculation by one of the authors (NVM) gave a value at the cascade maximum of  $5.8 \mu\text{rad}/10^{11}$  protons which is excellent agreement with both the data and the calculations presented here in detail.

Case C: For this case a longitudinal scan with verification of centering was made similar to that done for Case B with both the TEIR and HPI 1010 instruments. The data and the results of CASIM calculations using three different random number seeds are displayed on Fig. 11. The results of the calculations have been rebinned in the  $Z$  coordinate using the statistical errors calculated by the code as weights. As for Case B, the disagreements between the three calculations are representative of the statistical errors.

Contrary to Case B, the measurements typically exceed the CASIM calculations by factors of about three to four. In fact, as will be seen below, this is the only case

studied in which the measurements systematically exceeded the calculation. An independent calculation by one of the authors (NVM) yielded a value of  $0.9 \mu\text{rad}/10^{11}$  protons at the shower maximum which is consistent with the above calculations shown in detail. It was feared that the crack in the collimator (located in the vertical plane) was contributing additional absorbed dose not well modeled by the calculation. Also, since the shielding berm decreases in elevation downstream of Enclosure H perhaps skyshine of low energy neutrons emitted out of the end of the berm were also contributing to the measured absorbed dose but were not included in the calculation.

In order to test the above uncertainties, a similar test was done by closing the P-West collimator and bombarding it with a 400 GeV proton beam on March 4, 1981. The crack of the P-West collimator is in the horizontal plane so that (in contrast with the vertical crack in the P-Center collimator), the crack in the P-West case does not point toward the radiation instruments. The P-West collimator also slopes upward by 8 milliradians. Also, the absorbed dose was measured at the end of the berm. At the peak on top of the berm, absorbed dose rates of  $2.0 \mu\text{rad}/10^{11}$  protons were measured and rates 75% as large were measured on the end of the berm. The absorbed dose rates are thus a factor of two lower on top of the berm than in

the case of the P-Center collimator so that the crack may have some effect. Scaling the energy dependence would imply that only a 14 per cent effect is expected between 350 and 400 GeV. It seems doubtful that skyshine from the downstream areas is a significant contribution.

It is conceivable that P-Center measurement is sensitive to buildup of the cascade in the P-East and P-West collimators (not easily modeled) while the P-West collimator has a wall on one side of it. A calculation designed to test this effect by including all three collimators gave no evidence that this effect is significant.

It was found that a number of ground hog (Marmota monax) holes exist in this shielding berm with unknown locations under the position of the measurement. This could, of course, influence the measurement by reducing the actual quantity of shielding present. Such a reduction in shielding would probably not exceed 30 cm, but could conceivably increase the measured absorbed dose rate by as much as a factor of two. Such holes were not involved in any other case studied here.

This case exhibits some of the difficulties involved in modeling the geometry. This was the most difficult case to model of the four attempted here. It is the only case which

disagrees by more than a factor of two with the model prediction at the cascade maximum. We suspect, but have not proven conclusively, that the factor of four disagreement is a result of the vertical crack and the ground hog holes, neither of which enter into the model.

Case D: The data and calculations are displayed in fig. 12 in a manner similar to that used for Cases B and C. The results of the calculations have been rebinned as in Case C. As one can see, the agreement is quite good for  $z$  values between 0 and 300 cm, while at the peak and downstream the calculations usually exceed the measurement by about a factor of two. Again an independent CASIM calculation by one of the authors (NVM) gave a value of  $8.0 \mu\text{rad}/10^{13}$  protons at the cascade maximum which is quite consistent with the results shown in detail here. This case shows that reasonable results may be achieved even for very thick shields, especially if the geometry is simple and the beam targeting conditions are well understood.

A summary of the results of all four cases is given in table 1 where for each case the number of absorption lengths of lateral shielding between the target and the measurement (measured along the perpendicular to the beam axis), the measured absorbed dose rate, calculated absorbed dose rates, and ratio of measured to calculated doses at the cascade

maximum are listed.

#### 4. Conclusions

It is concluded that proper application of the Monte-Carlo code CASIM can predict absorbed dose within a factor of about three in situations where the geometry and beam loss mechanism are well understood. The differences between the calculations and measurements are not systematically correlated with shielding thickness. The agreement at the cascade maximum is quite good considering the uncertainties in the physics used in CASIM, in the geometry modeling, and in the absorbed dose measurements. In the two cases measured longitudinally beyond the cascade maximum, a tendency for absorbed dose rates to be overestimated by the code is indicated. It is obvious that more difficult cases than those studied here (e.g., scraping losses) would require great care in the modeling to achieve reliable results. In thick shields with "equilibrium" spectra other quantities of practical interest such as soil activation, energy deposition, and residual activation, should be predictable to roughly the same accuracy as seen

here in absorbed dose. However, specific experiments should be done to establish such a correspondence.

We would like to thank R. Dixon, S. Velen, S. Gronemeyer, and R. Rubinstein for their help in conducting these measurements and A. Van Ginneken for his helpful instruction in the use of CASIM and for his careful reading of the manuscript. The efforts of the instrument maintenance and calibration group at Fermilab are acknowledged.

## References

1. A. Van Ginneken, "CASIM (First Edition), Program to simulate Transport of Hadronic Cascades in Bulk Matter", Fermilab Report FN-272 (1975).
2. A. Van Ginneken and M. Awschalom, "High Energy Particle Interactions in Large Targets", Vol 1 (Fermilab, Batavia 1975).
3. M. Awschalom, S. Baker, C. Moore, A. Van Ginneken, K. Goebel, and J. Ranft, Nucl. Instr. and Meth. 138 (1976) 521.
4. M. Awschalom, P. J. Gollon, C. Moore, and A. Van Ginneken, Nucl. Instr. and Meth. 131 (1975) 235.
5. M. Hofert and C. Raffinsoe, Nucl. Instr. and Meth. 176 (1980) 443.
6. A. Van Ginneken, "Penetration of Prompt and Decay Muon Components of Hadronic Cascades Through Thick Shields", Fermilab Report TM-630.
7. Particle Data Group, Rev. Mod. Phys. 52 (1980) p 550.
8. P. J. Gollon, "Dosimetry and Shielding Factors Relevant to the Design of Iron Beam Dumps", Fermilab Report TM-664 (1976).
9. M. Awschalom, "Bonner Spheres and Tissue Equivalent Chambers for Extensive Radiation Monitoring Around a 1/2 TeV Proton Synchrotron", Proc. IAEA Symposium on Neutron Monitoring for Radiation Protection Purposes (Vienna, 1972) Vol 1, p 297.
10. Health Physics Instruments Model 1010, Health Physics Instruments, 1920 Chapala St., Santa Barbara, CA. 93101.

Table 1

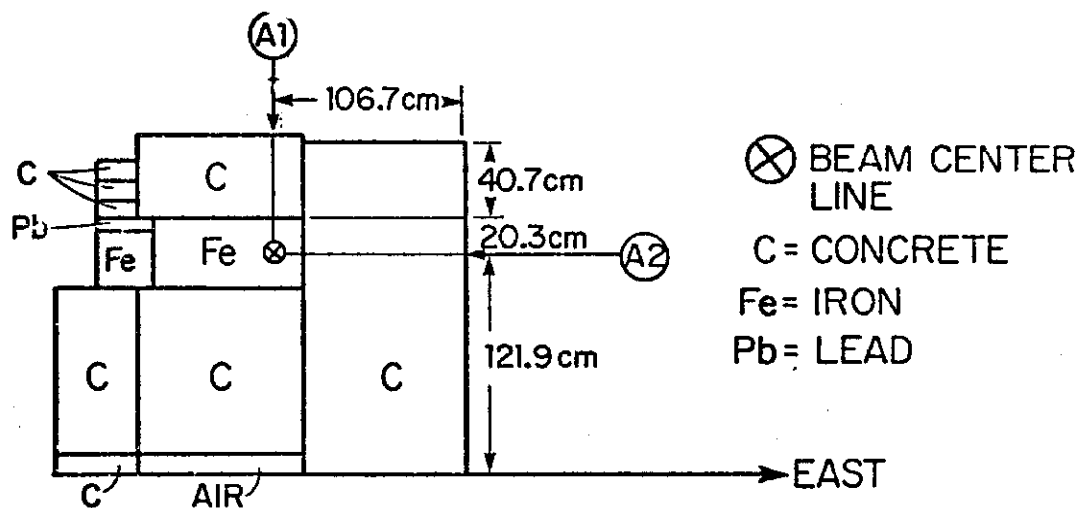
Results at Cascade Maxima

| Case | Number of Absorption Lengths <sup>†</sup> | Measured Absorbed Dose ( $\mu\text{rad}/10^{11}$ hadrons) | Calculated Absorbed Dose* ( $\mu\text{rad}/10^{11}$ hadrons) | Measured Dose / Calculated Dose |
|------|---|---|--|---------------------------------|
| A1   | 2.3                                       | $5.9 \times 10^5$   | $7.2 \pm 0.3 \times 10^5$                                    | 0.82                            |
| A2   | 3.3                                       | $2.6 \times 10^5$   | $2.6 \pm 0.7 \times 10^5$                                    | 1.00                            |
| B    | 12.1                                      | $5.5 \pm 0.5$   | $5.3 \pm 1.0$  | 1.03                            |
| C    | 14.3                                      | $4.0 \pm 0.5$   | $0.99 \pm 0.09$  | 4.04                            |
| D    | 17.3                                      | $(2.5 \pm 0.5) \times 10^{-2}$                            | $(4.3 \pm 0.3) \times 10^{-2}$                               | 0.58                            |

\*Averaged over all calculations described in detail here using statistical errors as weights for Cases B, C, and D.

<sup>†</sup>Ref. 7 was used to obtain these values.

CASE A  
VIEW FROM UPSTREAM



CASE A  
VIEW FROM EAST SIDE

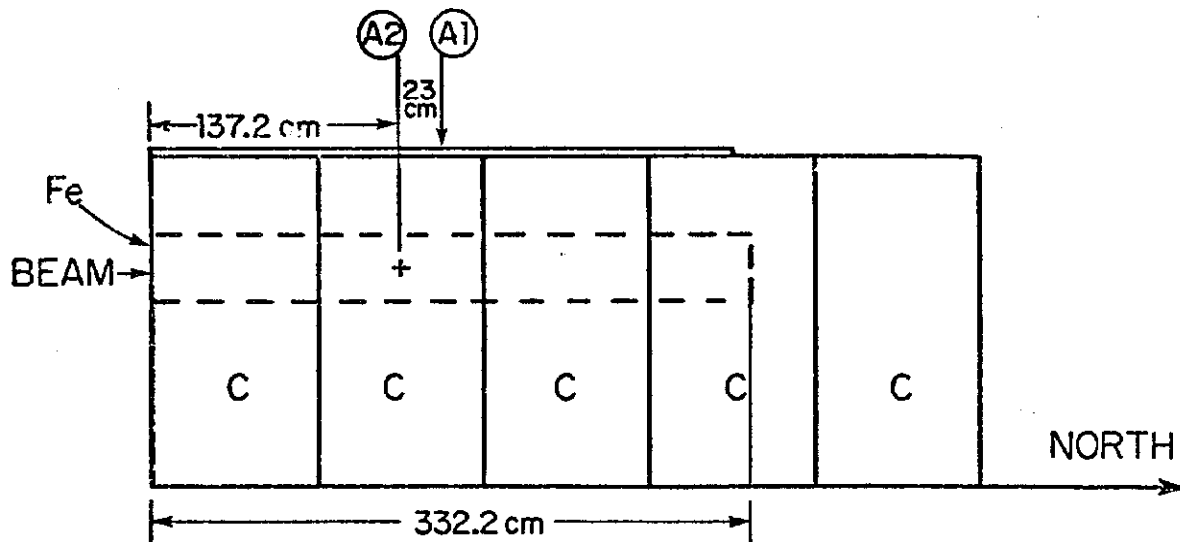


Figure 1

Case A: Two views of the actual shielding configuration. The beam is incident at 10 milliradians to the east of perpendicular.

CASE A (MODEL GEOMETRY)  
END VIEW  
(LOOKING DOWNSTREAM)

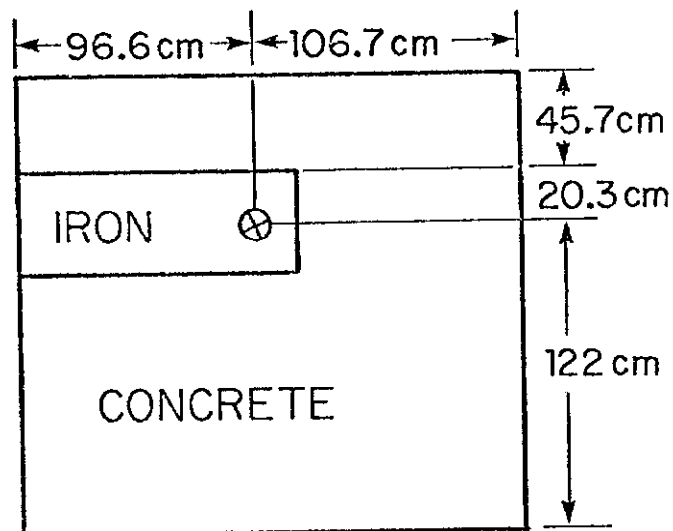
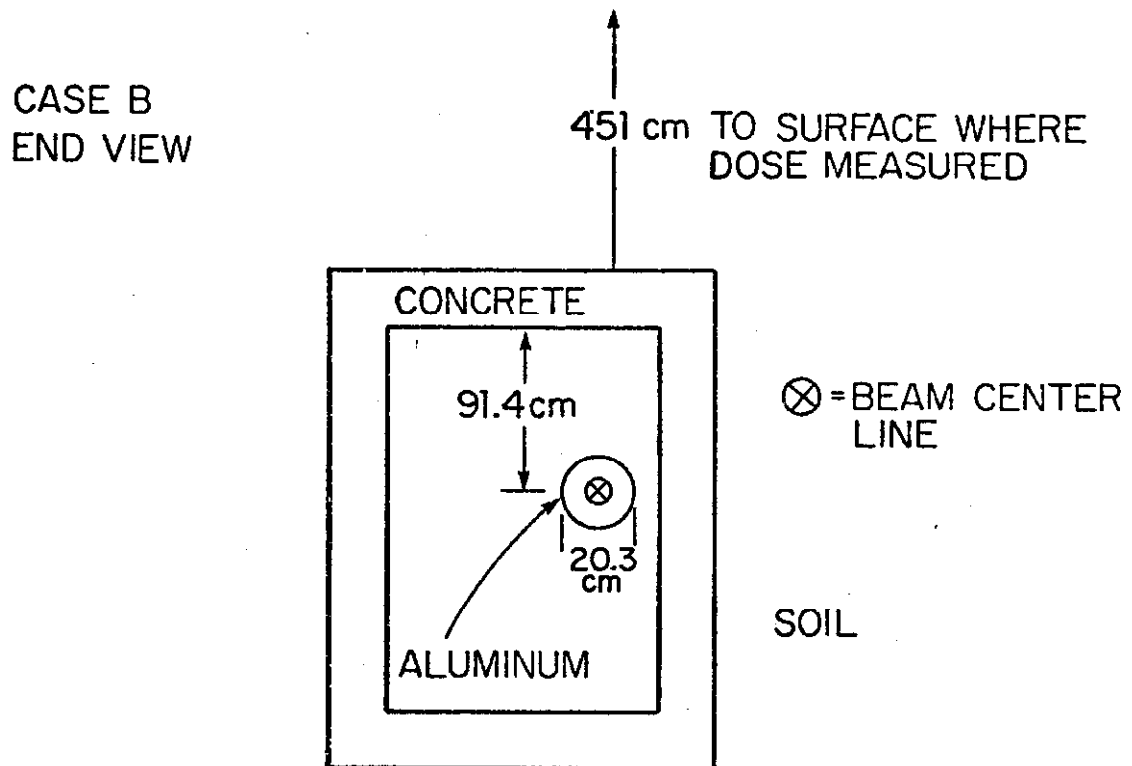


Figure 2

End view of the approximation to the Case A geometry used in the CASIM calculations. The iron was followed by concrete beyond a depth of 332 cm.



CASE B  
PLAN VIEW

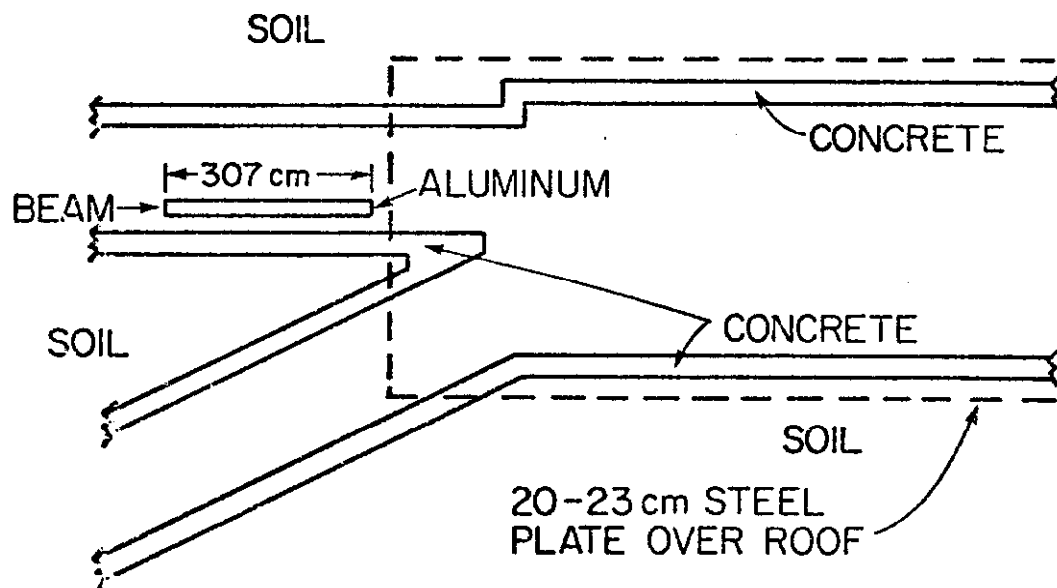
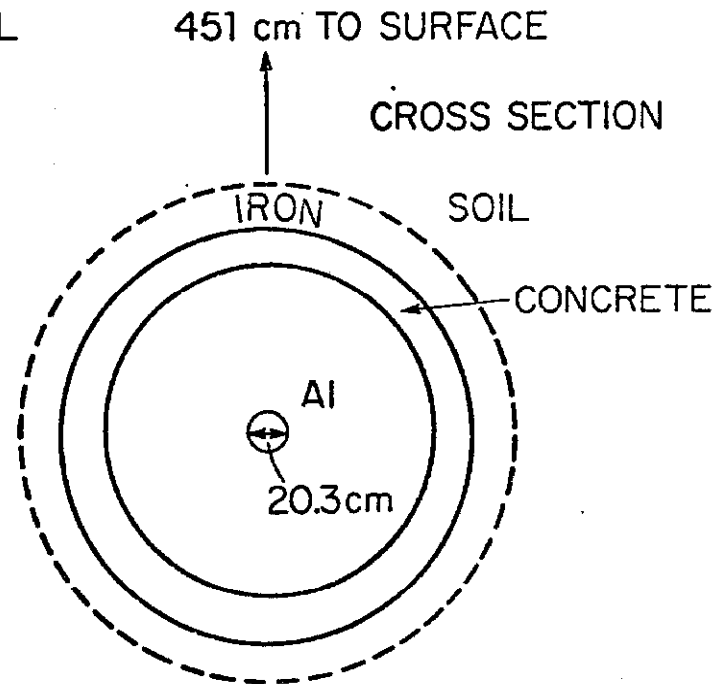


Figure 3

Case B: Two views of the actual shielding configuration.

CASE B  
MODEL



LONGITUDINAL SECTION

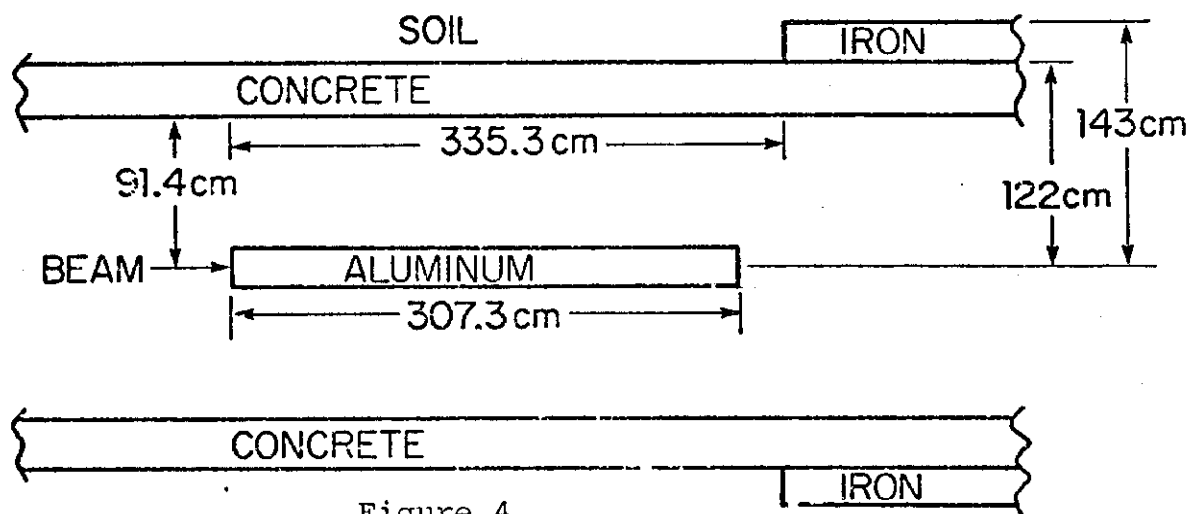
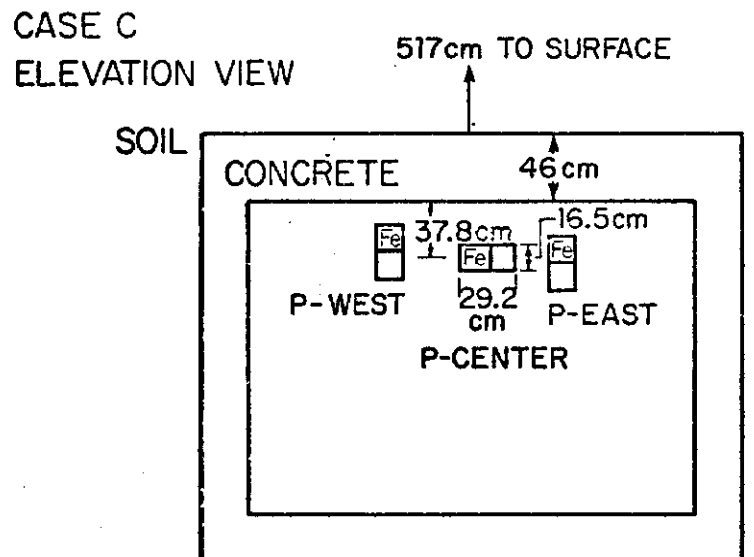


Figure 4

Two sections of the approximation to the geometry of Case B used in the calculations.



NOTE: OUTER SHEET METAL JACKETS OF COLLIMATORS NOT SHOWN

CASE C  
PLAN VIEW

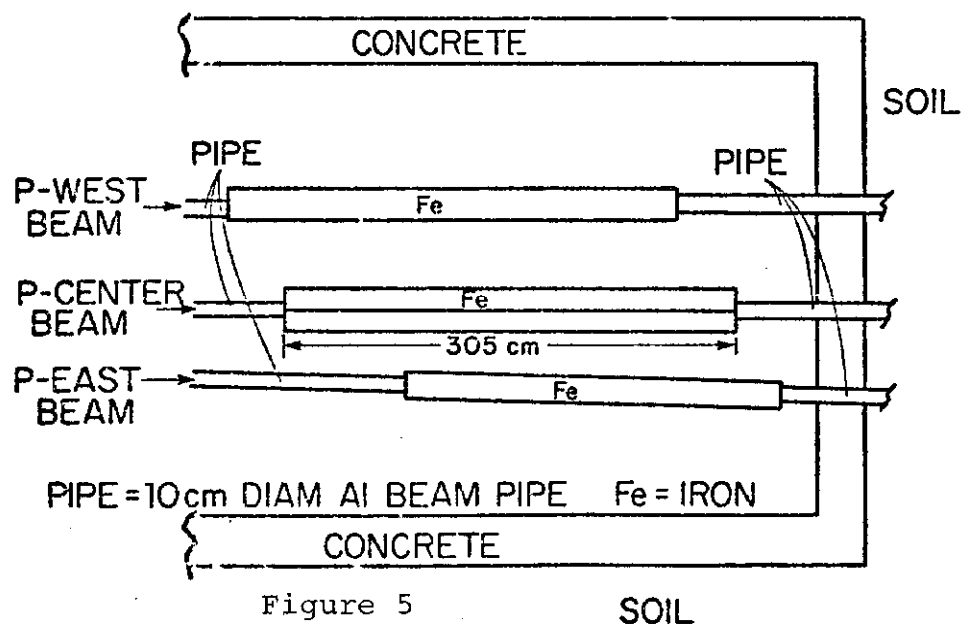


Figure 5

SOIL

Case C: Two views of the actual shielding configuration. Outer sheet metal jackets of collimators are not shown.

CASE C TARGET MECHANISM  
P-CENTER BEAM

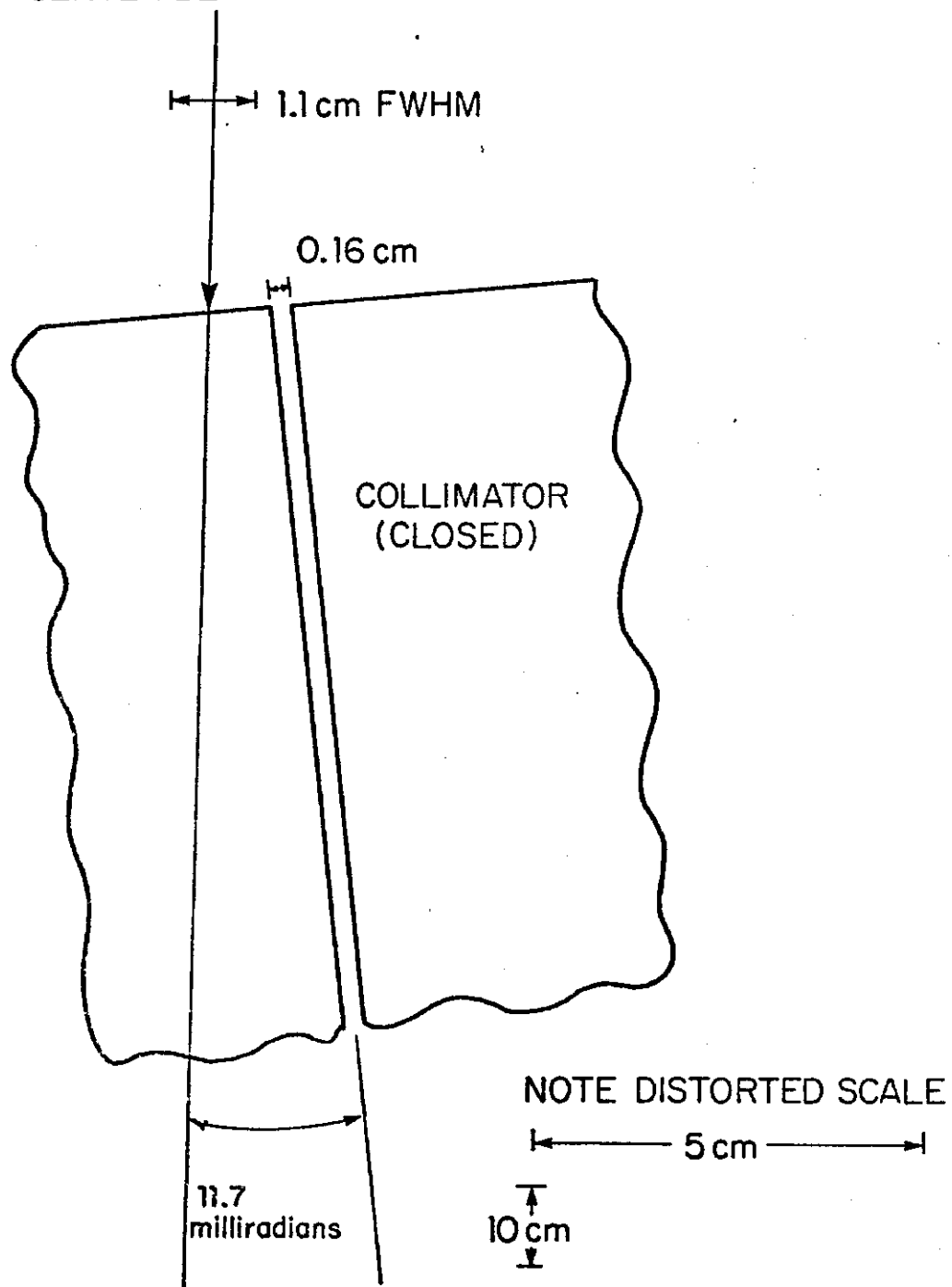


Figure 6

Detailed view of targeting geometry of Case C.

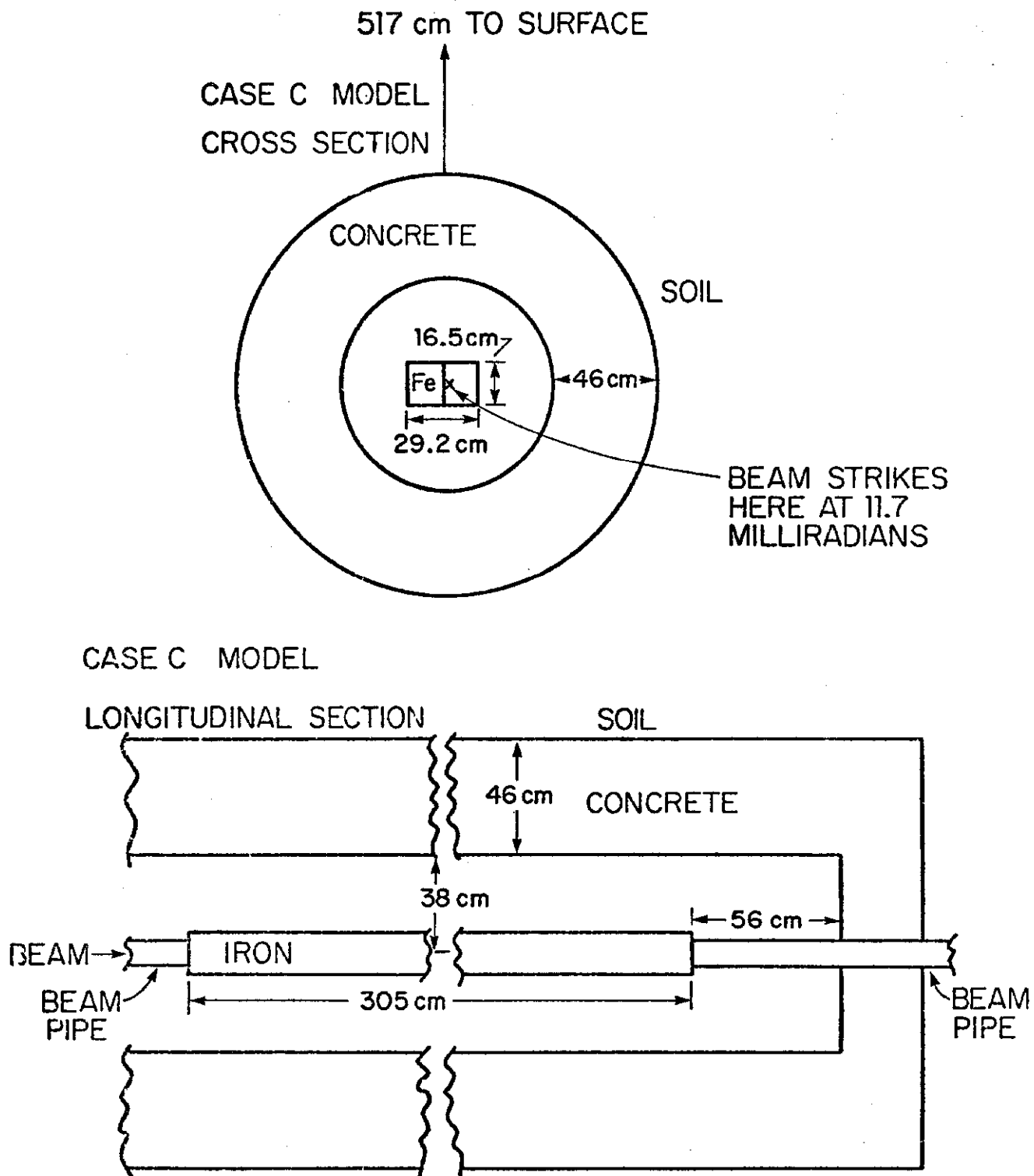
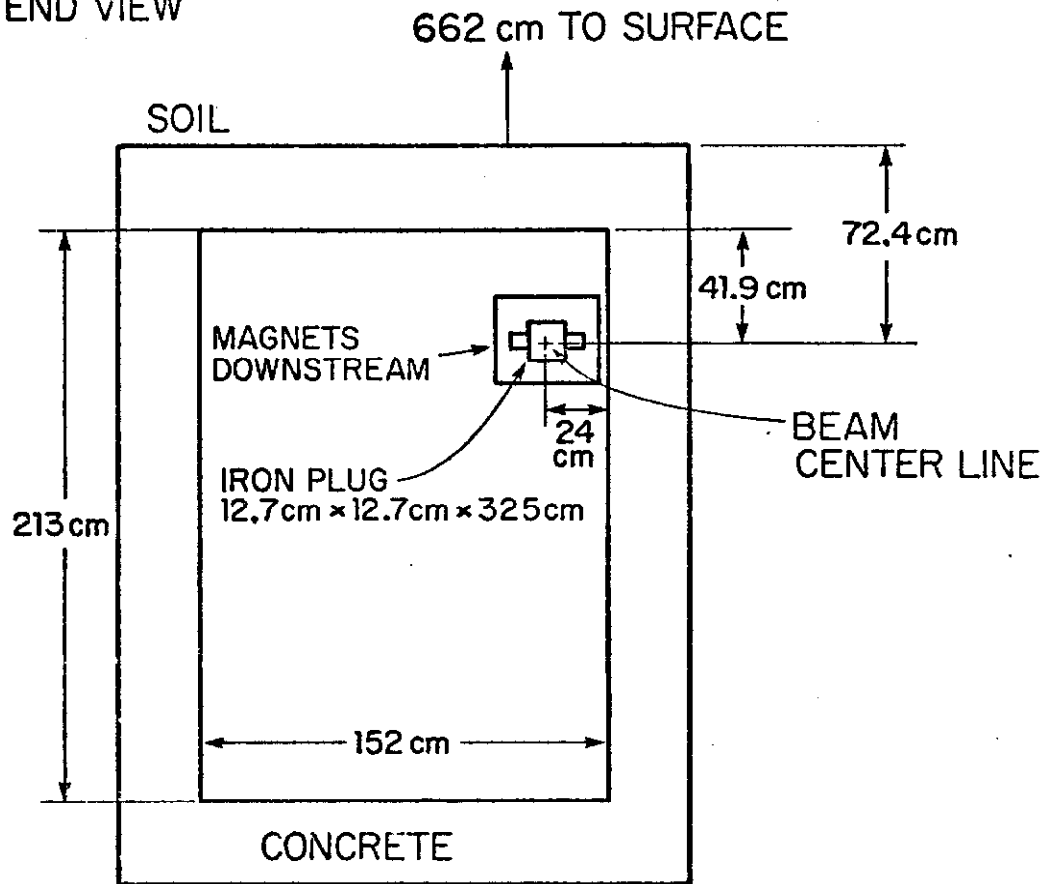


Figure 7

Two sections of the approximations to the geometry of Case C used in the CASIM calculations.

CASE D  
END VIEW



CASE D

SIDE VIEW

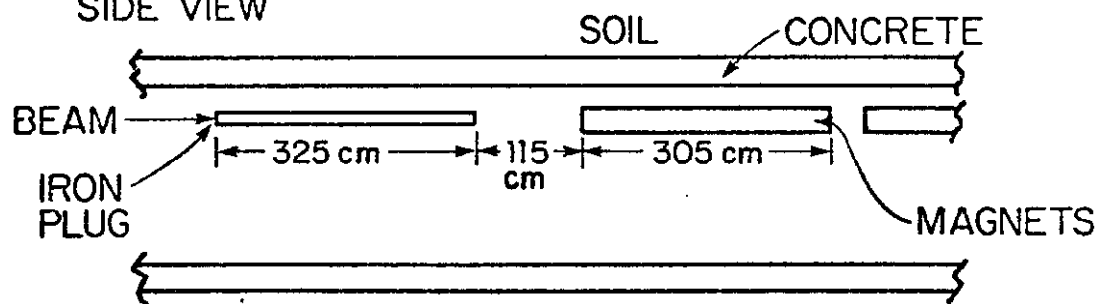


Figure 8

Case D: Two views of the actual shielding configuration.

CASE D MODEL  
END VIEW

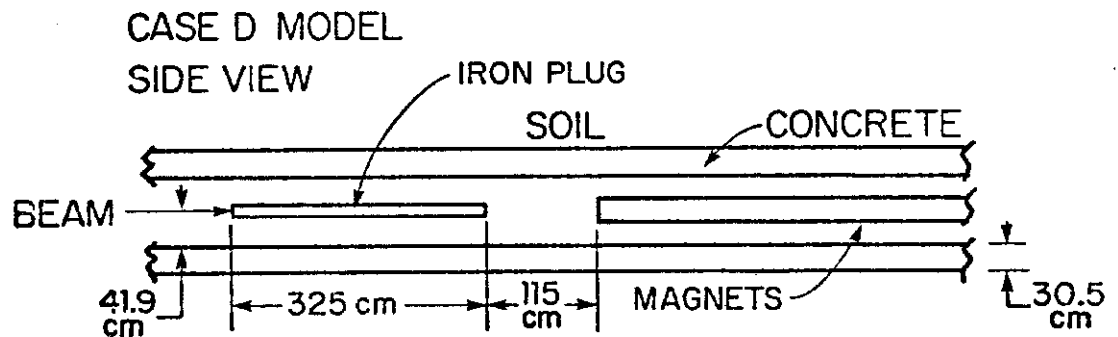
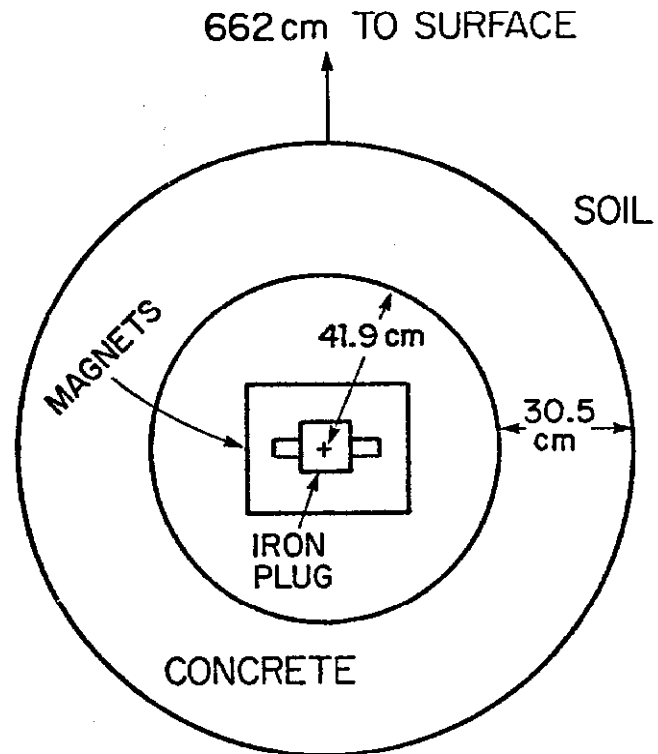


Figure 9

Two views of the approximation to the geometry of Case D used in the CASIM calculations.

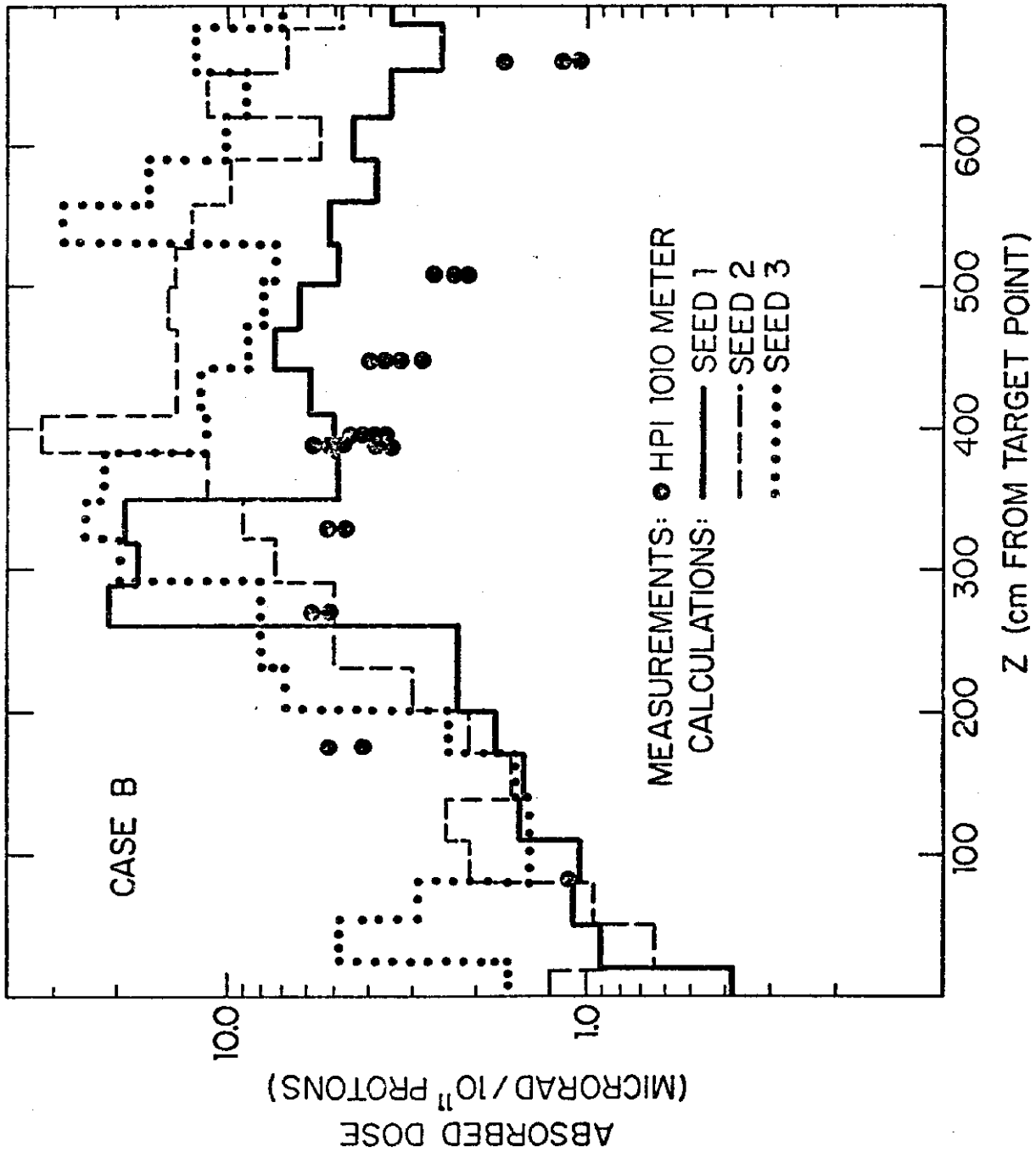


Figure 10

Case B: CASIM calculations and absorbed dose measurements plotted as a function of longitudinal coordinate Z.

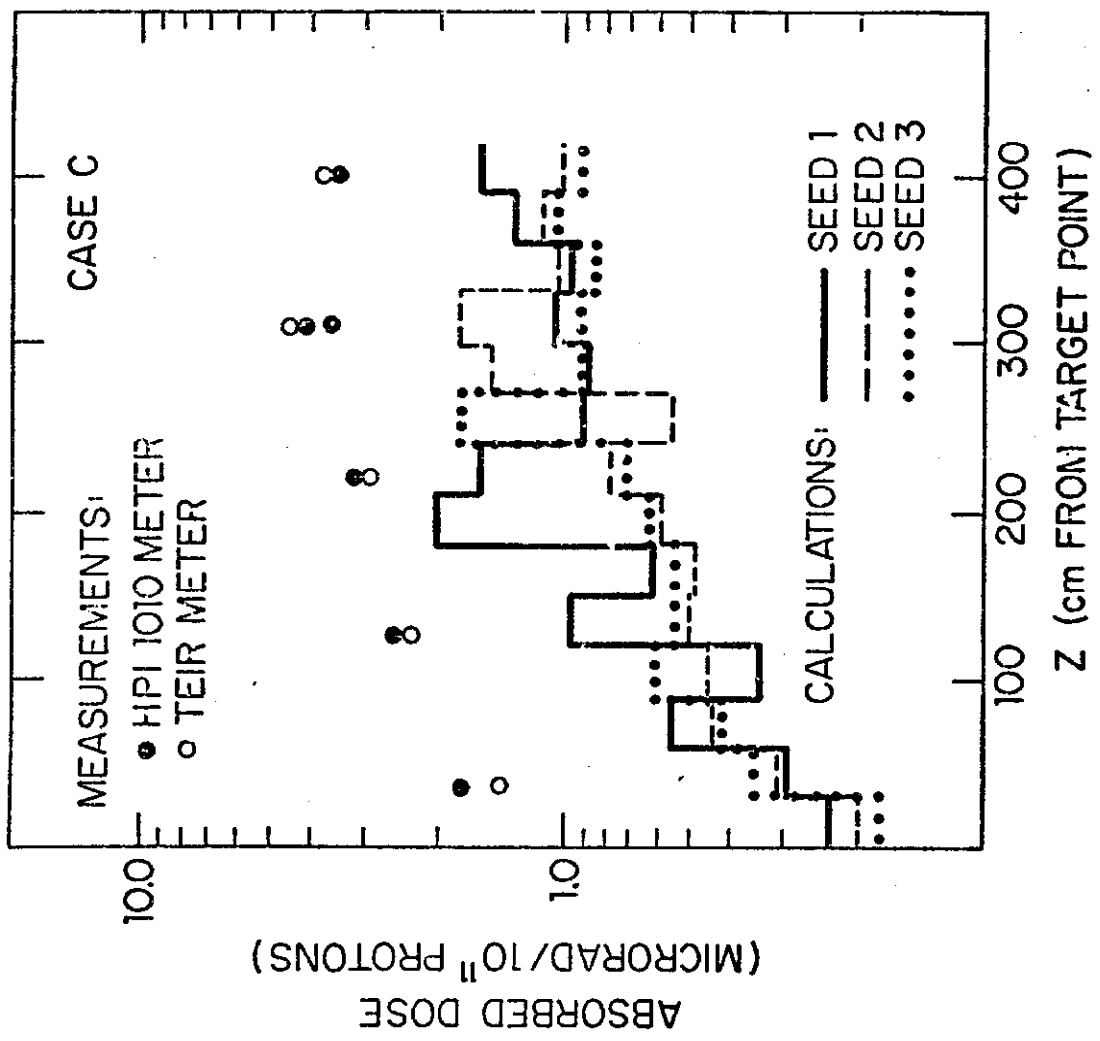


Figure 11

Case C: CASIM calculations and absorbed dose measurements plotted as a function of longitudinal coordinate Z.

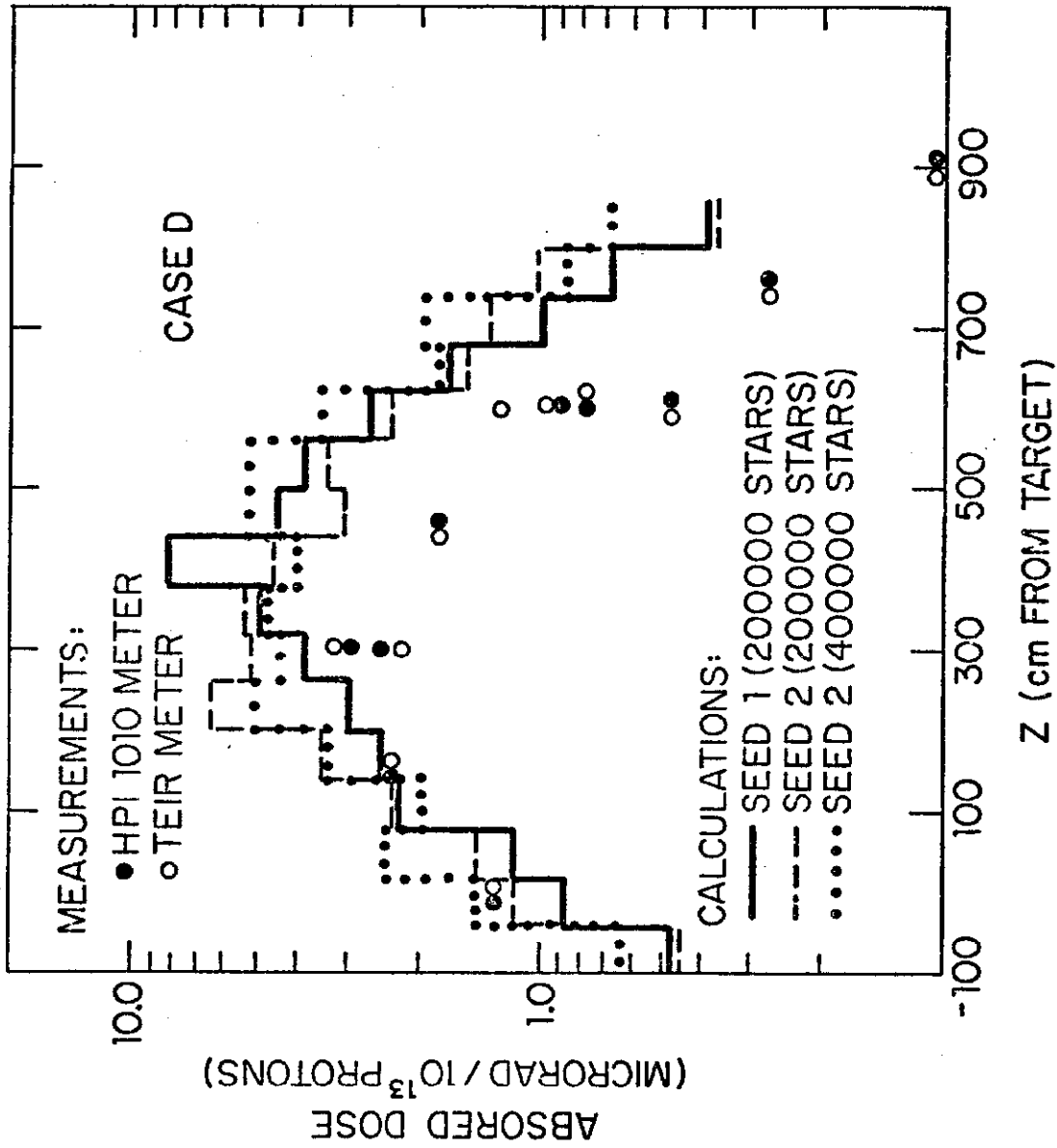


Figure 12

Case D: CASIM calculations and absorbed dose measurements plotted as a function of longitudinal coordinate Z.